Soft Matter

PAPER

View Article Online
View Journal | View Issue

Cite this: *Soft Matter*, 2016, 12, 817

DNA translocation through single-layer boron nitride nanopores†

Zonglin Gu,‡[a] Yuanzhao Zhang,‡[b] Binquan Luan[b] and Ruhong Zhou*[abc]

Received 1st September 2015,
Accepted 27th October 2015

DOI: 10.1039/c5sm02197a

www.rsc.org/softmatter

Ultra-thin nanopores have become promising biological sensors because of their outstanding signal-to-noise ratio and spatial resolution. Here, we show that boron nitride (BN), which is a new two-dimensional (2D) material similar to graphene, could be utilized for making a nanopore with an atomic thickness. Using an all-atom molecular dynamics simulation, we investigated the dynamics of DNA translocation through the BN nanopore. The results of our simulations demonstrated that it is possible to detect different double-stranded DNA (dsDNA) sequences from the recording of ionic currents through the pore during the DNA translocation. Surprisingly, opposite to results for a graphene nanopore, we found the calculated blockage current for poly(A–T)$_{40}$ in a BN nanopore to be less than that for poly(G–C)$_{40}$. Also in contrast with the case of graphene nanopores, dsDNA models moved smoothly and in an unimpeded manner through the BN nanopores in the simulations, suggesting a potential advantage for using BN nanopores to design stall-free sequencing devices. BN nanopores, which display several properties (such as being hydrophilic and non-metallic) that are superior to those of graphene, are thus expected to find applications in the next generation of high-speed and low-cost biological sensors.

Introduction

Reliably detecting single molecules has been the focus of many researchers in the past decade.[1–5] Achieving such detection will change the landscape of many aspects of science and industry. One prominent example is next-generation DNA sequencing, for which the ability to detect single molecules will yield a much higher sequencing speed and a significant lower cost than the current-generation technology. The fundamental idea[2,6] is to simultaneously thread single-stranded DNA through a protein nanopore in a single-file format and detect sequence-dependent ionic currents through the pore. For synthetic solid-state nanopores, due to their large sizes, efforts have been focused on sequencing modified[7] or converted[8] double-stranded DNA (dsDNA).

One major challenge faced by all DNA sequencing technologies based on solid-state nanopores is to achieve a high signal-to-noise ratio as well as high spatial resolution in order to distinguish the types of DNA bases or base pairs. This requires the thickness of the nanopore to be comparable with the stacking distance of the DNA base pair, which lies in the sub-nanometer regime. Thus, the ultrathin nanopore has emerged as a promising candidate for this purpose.[9–12] Such a nanopore is typically drilled on a solid membrane separating two (*cis* and *trans*) fluidic chambers. A biasing voltage across the membrane is then applied to drive the DNA through the pore. During the translocation, DNA physically blocks the pore to different characteristic degrees, yielding a blockage of ionic currents,[13–15] which can provide information about the physical characteristics (*e.g.*, size and charge) of the transported DNA. Thus, depending on the types of nucleotides passing through the one-layer pore, time-dependent current signatures could ideally be used to recover information about the DNA sequence.

Graphene is perhaps the best-known material that meets the above-described requirement for pores, and indeed there have been extensive experimental and theoretical investigations on using graphene as a novel nanopore sensor.[9,10,16,17] However, when applied to DNA sequencing, graphene-based nanopores suffer from a few drawbacks, with the most serious three being the adherence of DNA to graphene, low functional yield, and considerable noise. Graphene is highly hydrophobic and very 'sticky' to the DNA strand, and can hence trap DNA during its translocation,[17] especially under the low biased voltage required for reliable sequencing. This hydrophobicity together with the pinholes (defects) introduced during the manufacturing process contribute to the much higher noise level in graphene nanopores when compared with more traditional silicon nitride nanopores.[10]

[a] *School for Radiological and Interdisciplinary Sciences (RAD-X) and Collaborative Innovation Center of Radiation Medicine of Jiangsu Higher Education Institutions, Soochow University, Suzhou, 215123, China*
[b] *Computational Biological Center, IBM Thomas J. Watson Research Center, Yorktown Heights, NY 10598, USA. E-mail: ruhongz@us.ibm.com*
[c] *Department of Chemistry, Columbia University, New York, NY 10027, USA*
† Electronic supplementary information (ESI) available. See DOI: 10.1039/c5sm02197a
‡ These authors contributed equally.

Boron nitride (BN), also called white graphene, is composed of alternate boron and nitrogen atoms in a honeycomb structure. It is just as thin as graphene, and is a fantastic nanomaterial since it displays most of the extraordinary electrical and mechanical properties that graphene displays. Moreover, it is less hydrophobic than graphene, which can minimize the hydrophobic interaction that impedes the DNA translocation. It also shows other advantages over graphene in terms of its insulating property in high-ionic-strength solution and fewer defects made during the manufacturing process. All the above properties suggest BN to be a very promising candidate for nanopore devices, which has already been demonstrated in a very recent experimental study.[18]

To further evaluate properties (diameters and thickness) of BN nanopores for DNA sequencing and/or sensing, we here report studies of dsDNA translocation through BN nanopores using large-scale molecular dynamics (MD) simulations,[19–21] which can provide atomic details of the transport process. MD simulations have previously been successfully applied to studies of a wide range of phenomena, such as interactions between biomolecules and nanomaterials,[22,23] protein folding,[24–26] nanodevice development[27–29] and nanotoxicity.[30] We investigated the influence of pore size, magnitude of the bias voltage, number of BN layers, and, most importantly, the composition of dsDNA on the signal of the ionic current during the DNA translocation through the BN nanopore. Elucidating the effect of these factors is crucial for the design of next-generation BN-pore-based DNA sequencing devices.

Results and discussion

Fig. 1 shows the initial setup of a typical current simulation system that we employed. A double-stranded DNA molecule, such as poly(G–C, A–T)$_{20}$, poly(A–T)$_{40}$, or poly(G–C)$_{40}$ (see ESI,† Table S1 for more sequence information), was placed right above the BN pore. The complex was then solvated in a 1 M KCl electrolyte, which minimized the electrostatic interaction between dsDNA and the charged boron and nitrogen atoms in the BN pore due to the strong screening effect.[31] The size of the simulation system was made large enough so that the distance between molecules related by mirror symmetry (due the periodic boundary conditions) was much larger than the Debye screen length for the 1 M KCl electrolyte. Also the cross-sectional area of the entire BN nano-sheet was modeled to be much larger than that of a nanopore, guaranteeing confinement of the electric field mainly to the region above the nanopore (similar to the experimental condition). We studied the sequence-dependent DNA transport through BN nanopores with various diameters D and thicknesses. A detailed list of the MD simulations that we ran is found in Table S1 (ESI†).

To characterize the ionic current flow through the BN nanopore, we first performed simulations A1–A5 in Table S1 (ESI†) (without any dsDNA) to measure the relationship between the open-pore conductance and the pore diameter (Fig. 2). Five systems with pore diameters ranging from 2.5 nm to 6.5 nm

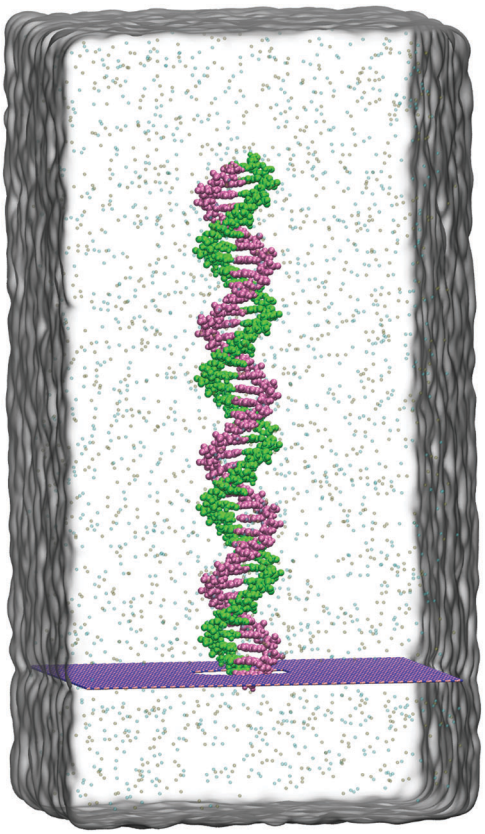

Fig. 1 Initial setup of a BN nanopore–dsDNA system. The dsDNA (colored in magenta and green) is placed right above the BN nanopore, and perpendicular to the BN sheet (colored purple). K^+ and Cl^- ions are shown as hollow brown and cyan dots, respectively. Also shown in grey is the water surface at the boundary of the periodic cell.

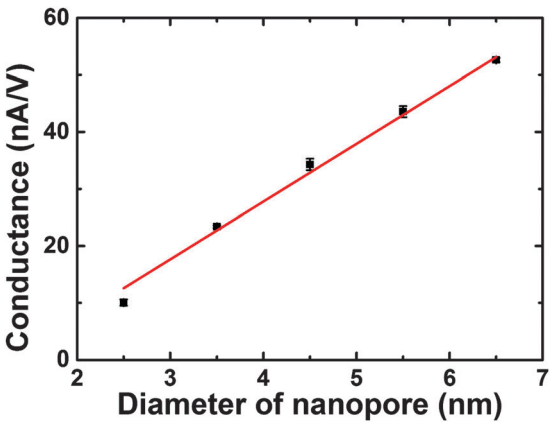

Fig. 2 Conductance of the BN nanopore as a function of its diameter. The data can be fitted very well with a straight line for the range of pore diameters investigated.

were simulated, each subjected to 1.0 V of external voltage, which drove K^+ and Cl^- ions through the pore in opposite directions. The conductance was measured as $\frac{\langle I \rangle}{V}$, with $\langle I \rangle$ being the average ionic current through the pore. We found that the pore conductance increased linearly with the pore diameter.

Because of the peculiar aspect ratio between the pore diameter and pore thickness, the access resistance is more significant than the pore resistance, resulting in the linear relationship. This linear dependence between conductance and diameter is indeed in qualitative agreement with previous theoretical results[12] on an atomically thin nanopore and experimental data on a graphene nanopore.[9]

After the above initial characterization of the BN pores, we added dsDNA to the system (as shown in Fig. 1, and simulations B1–B5 in Table S1 (ESI†) with poly(G–C, A–T)$_{20}$) to study the translocation kinetics of the dsDNA through the BN nanopore, and how the pore diameter affects the change in current caused by the blockage of the pore by the dsDNA (namely blockage current). The dsDNA was placed vertically right above the mouth of the pore at the beginning of all simulations, and the bias voltages were again set to 1.0 V. Fig. 3a–e show the time evolution of the ionic current and the center of mass (COM) of the dsDNA moving along the z direction during the translocation, with increasing pore sizes. As expected, the blockage effect was found to be most pronounced for small pores, where dsDNA can occupy most of the cross-sectional area of the pore during the translocation and result in a significant blockage. As the pore size was increased, both the blocked (dashed grey lines in Fig. 3) and open-pore currents (dashed green lines in Fig. 3) increased. However, not only did the ratio between these two currents approach unity, the absolute difference between them also dropped sharply, from around 9 nA for the 2.5 nm (in diameter) pore to around 2 nA for the 6.5 nm-diameter pore. This drop is due to the cross-sectional area of the 6.5 nm-diameter pore being much larger than that of a DNA molecule (with a diameter D_{DNA} of $\sim$2 nm), resulting in a much less effective blockage in larger pores. The percentage of the current being blocked, *i.e.*, $(D_{DNA}/D)^2$, was estimated to be $\sim$10% for the 6.5 nm-diameter pore, which is consistent with results shown in Fig. 3e. Generally, smaller nanopores can yield a higher sensitivity, and hence provide better resolution for DNA sequencing.

In previous studies, the translocation of dsDNA through graphene nanopores was observed to suffer from serious adhesion to the graphene membrane under similar bias voltages used here,[16] primarily due to the strong hydrophobic interaction between the DNA bases and the graphene membrane. This adhesion can result in a critical slowing down of the sequencing, and even in dsDNA becoming stuck in the middle of the translocation, thus damaging the pore. It is therefore interesting to determine how the BN nanopore compares with the graphene nanopore in this regard. As shown in Fig. 3, the dsDNA COM changed uniformly with time until the dsDNA exited the pore for all of the pore sizes simulated, suggesting the dsDNA moved at a nearly constant velocity during the translocation even for the very small (2.5 nm in diameter) pore. Visual analysis of the translocation from movies in ESI† (Movie S1–S3) further confirmed this observation of dsDNA moving smoothly and in an unimpeded manner through the BN nanopore. This result directly contrasted with the case of the graphene nanopore, and suggests a potential advantage for BN nanopores in designing stall-free sequencing devices.

Having demonstrated the effects of different-sized BN nanopores on the kinetics and blockage current during the dsDNA translocation through these nanopores, we further carried out simulations of poly(A–T)$_{40}$ and poly(G–C)$_{40}$ permeating through a 2.5 nm-diameter pore (simulations C1–C5 and D1–D5 in Table S1, ESI†). Using these simulations, we evaluated the ability of the

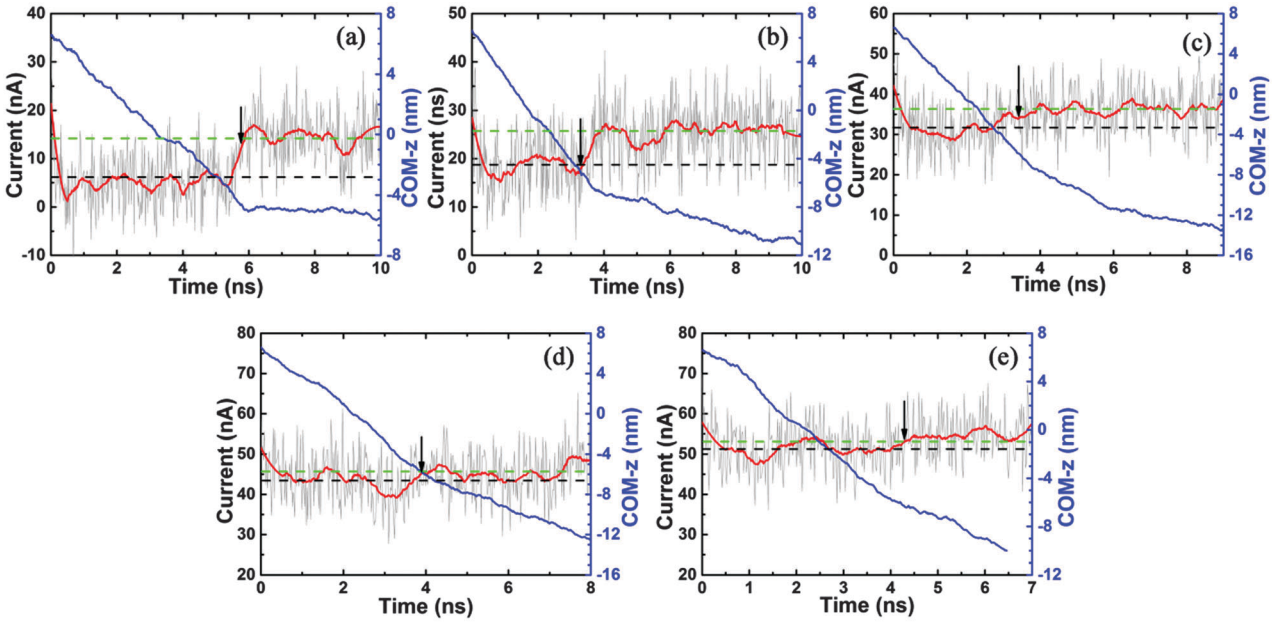

Fig. 3 Time evolution of ionic current (red curve) and the center of mass (COM) of the dsDNA along the z axis (blue curve) when transported through nanopores with diameters of (a) 2.5 nm, (b) 3.5 nm, (c) 4.5 nm, (d) 5.5 nm and (e) 6.5 nm (B1–B5 in Table S1, ESI†). The arrows indicate the moments when the dsDNA exited the nanopore. The green and black dashed lines are the mean values of the open pore and blockage currents in each system.

BN nanopore to distinguish A–T and G–C base pairs under different voltages, and hence assessed the potential of BN-nanopore-based DNA sequencing. The difference between the signals from the A–T and G–C base pairs was significantly reduced for the above-mentioned larger pores, because such pores yield a smaller ratio of the cross-sectional area of dsDNA to that of the pore, and this ratio determines the current blockage.

The currents of poly(A–T)$_{40}$ and poly(G–C)$_{40}$ clearly differed from each other for the range of biasing voltages studied, with the difference most pronounced at 1 Volt, while has a worst separation at 1.5 Volt (Fig. 4a). For comparison, we did not find a clear difference in simulated currents for the same-sized graphene pore (Fig. S1, ESI†), likely due to the hydrophobicity of the graphene pore, which promotes the local stretching of dsDNA. Fig. S1 (ESI†) suggests that poly(A–T) $_{40}$ and poly(C–G)$_{40}$ were equally stretched in the hydrophobic graphene pore. In an independent simulation, we found that dsDNA was broken and stuck near the graphene pore, *i.e.*, the hydrophobic base-stacking in dsDNA became replaced by hydrophobic stacking of DNA bases on the graphene surface (Fig. S2, ESI†). Note that it was critical to use a relatively high concentration of 1 M electrolyte here; otherwise, the pore radius would be less than the sum of the DNA radius and the Debye screening length at low electrolyte concentrations (*e.g.*, 1 nm for a 0.1 M electrolyte) and thus counterions of DNA (that contribute significantly to the pore current) would be excluded by the pore. On the other hand, the base-pair velocity of the poly(A–T)$_{40}$ was a bit faster than that of poly(G–C)$_{40}$ above a 0.8 V bias voltage, but unlike the blockage currents, the velocities of these two DNA polymers were not different enough to serve as a reliable indicator (Fig. 4b).

To provide a detailed look at the process, we plotted the mean numbers of heavy atoms from poly(A–T)$_{40}$ and poly(G–C)$_{40}$ that were in the nanopore during the translocation, which translates into the relative area of the dsDNA cross section in the pore (Fig. 4c). Fig. 4c reveals the molecular origin of base-pair detection: different degrees of stretching experienced by G–C and A–T under stress. In Fig. S3 (ESI†), we show poly(G–C)$_{40}$ to be more flexible than poly(A–T)$_{40}$ and thus easier to be stretched. The non-uniform distribution of the electric field around the pore[32] apparently induced stress on the section of dsDNA within the pore, stretching it to a certain degree. A previous study showed poly(G–C)$_{40}$ to be softer than poly(A–T)$_{40}$ under identical stress,[33]

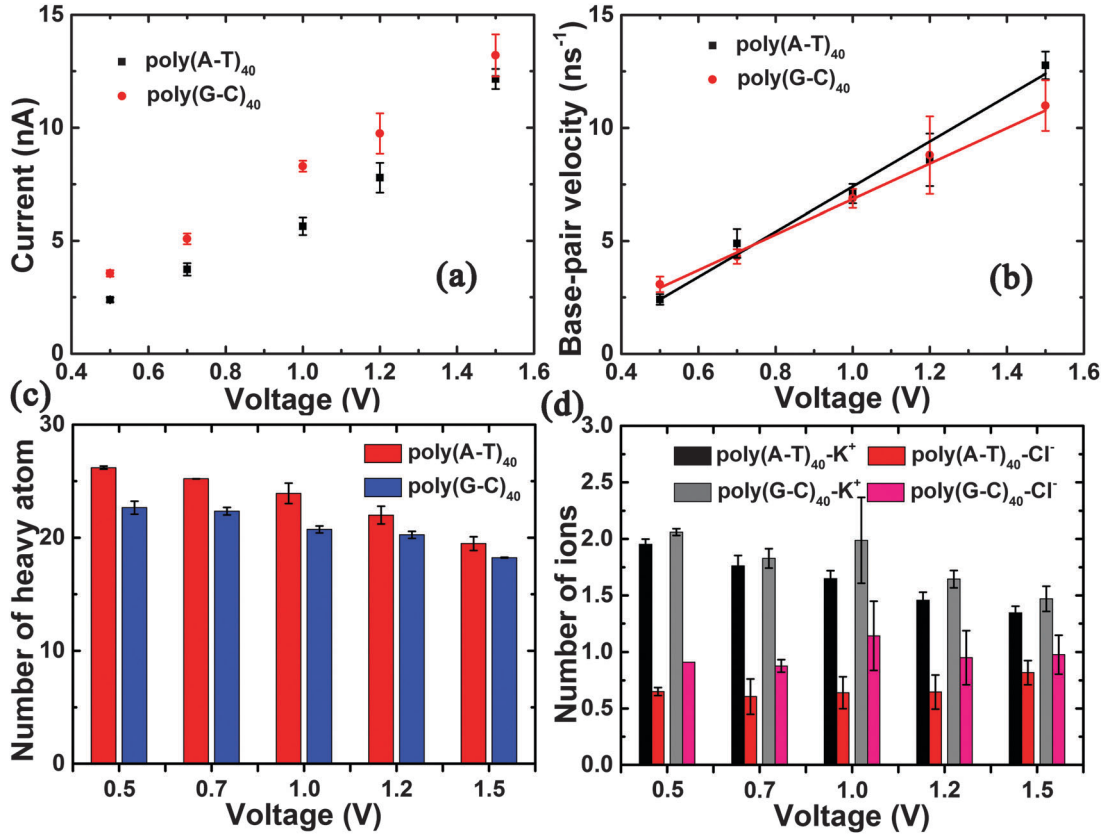

Fig. 4 (a) The blockage currents of poly(A–T)$_{40}$ and poly(G–C)$_{40}$ being transported through a 2.5 nm-diameter nanopore under different voltages. The differences between their currents were significant for all the voltages studied, except the largest at 1.5 V. (b) Base-pair velocities of poly(A–T)$_{40}$ and poly(G–C)$_{40}$ permeating through the same pore under different voltages. The differences between their velocities were not significant, and hence such a velocity measure is not a good indicator of the identity of the base pair. (c) The mean heavy atom number of poly(A–T)$_{40}$ and poly(G–C)$_{40}$ near the nanopore during translocation (defined as the number of heavy atoms whose van der Waals (VDW) spheres interact with the pore on the *z* axis). It can be inferred that poly(G–C)$_{40}$ was constantly more stretched than poly(A–T)$_{40}$ during permeation under all voltages studied, which explains the higher current blockage induced by poly(A–T)$_{40}$. (d) The mean number of K^+ and Cl^- ions close to the BN nanopore, *i.e.*, within 1.25 nm of the central axis of the BN nanopore and within 0.4 nm of the BN sheet.

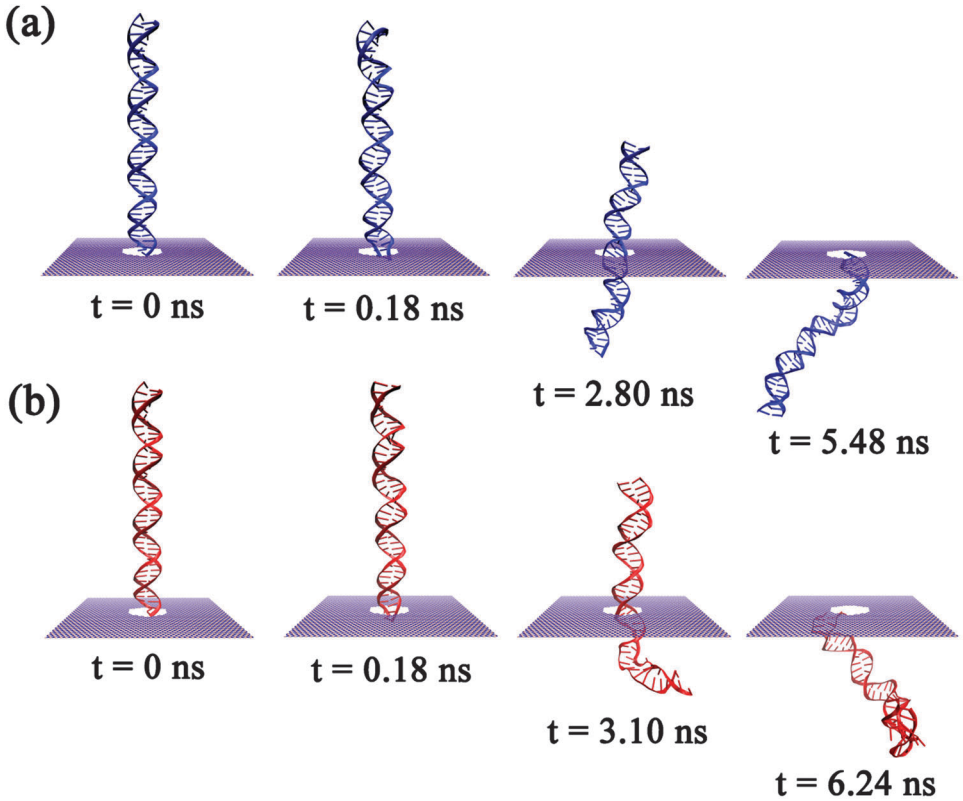

Fig. 5 Representative snapshots of poly(A–T)$_{40}$ (a) and poly(G–C)$_{40}$ (b) being driven through a 2.5 nm-diameter nanopore by a 1.0 V bias voltage. The four snapshots in each trajectory represent the dsDNA at its initial configuration, as it started entering the nanopore, halfway through the pore, and exiting the pore.

and thus would adopt a more stretched configuration with a smaller cross section, allowing more ions to pass through the pore. Similar to our simulation results, experimental studies also demonstrated the blockage current in a silicon-nitride nanopore for a poly(A–T) homopolymer to be less than that for a poly(G–C) homopolymer.[34] In contrast, previous MD studies showed that the blockage current of poly(A–T)$_{40}$ was higher than that of poly(G–C)$_{40}$ when transported through a graphene nanopore, likely due to the different interaction between DNA and the graphene nanopore, as well as the different orientation of DNA in the graphene nanopore, as compared to those with the nitride nanopores.

We also showed the mean number of K^+ and Cl^- ions around the BN nanopore, defined as the ions within 1.25 nm of the central axis of the BN nanopore and not farther away than 0.4 nm from the BN sheet (Fig. 4d). The number of K^+ ions and of Cl^- ions around the pore were calculated to be consistently higher in the poly(G–C)$_{40}$ systems than in the poly(A–T)$_{40}$ systems, with the largest margin occurring under 1 Volt of bias voltage. These results agree well with the results in Fig. 4a, and also suggest that the difference in the magnitudes of the current magnitude derived from both ions.

Four snapshots of the translocation process are shown in Fig. 5 for poly(A–T)$_{40}$ and for poly(G–C)$_{40}$ under 1 V bias voltage. The poly(A–T)$_{40}$ was calculated to travel a bit faster than poly(G–C)$_{40}$, but both types of dsDNA permeated smoothly, without sticking or adhering to the membrane. The third panel of Fig. 5a or b highlights the stretching of the DNA segment near the pore as mentioned above, with the poly(G–C)$_{40}$ showing more stretching.

Conclusion

Using MD simulations, we have demonstrated that BN nanopores can yield high-quality signals of ionic currents. When recording the current of the pore, it was desirable to maximize the difference (signal) between the open-pore current and the blockage current. To achieve such a difference, which can be estimated as $I_{open}(D_{DNA}/D)^2$, one could make a small pore (*i.e.* $D_{DNA} \sim D$) and/or increase the open-pore current. The latter requires a reduction of the pore resistance or of the pore length. In our simulations, the BN pore was atomically thin, which minimized the pore resistance. Our simulation results showed a linear relationship between the conductance and the pore radius, which consistently indicated the pore resistance to be much less than the access resistance.

Additionally, we found that the blockage current can be very sensitive to the DNA sequence near the pore, also due to the atomically thin pore. Because of the sequence-dependent DNA elasticity, the poly(A–T)$_{40}$ and poly(G–C)$_{40}$ homopolymers were not equally stretched by the non-uniform electric fields near the BN pore. The different extents to which poly(A–T)$_{40}$ and poly(G–C)$_{40}$

were stretched resulted in different reductions of the cross-sectional area of the homopolymers, which yielded different blockage currents. While not studied in this work, we expect that other DNA sequences (designed with different levels of elasticity) might yield distinct currents as well. Therefore, these electric signals can be used to monitor the local sequence/structure of DNA.

It was shown in a previous experiment[8] that instead of sequencing a flexible ssDNA in a solid-state nanopore, one can sequence a dsDNA molecule that is chemically and biologically converted from the ssDNA. Inspired by this concept, it is possible to consider translating each nucleotide type in ssDNA to one designed dsDNA segment (*e.g.*, poly(A–T)$_{10}$) in a converted dsDNA molecule. The key idea here is to detect a much larger dsDNA segment instead of just one nucleotide, which is still very challenging for a synthetic nanopore. Since the blockage current of the dsDNA was shown to be sequence dependent in our simulation and previous experiment,[34] the original sequence of the ssDNA can be derived from recording the current in the BN pore, thus suggesting a potentially new method for DNA sequencing.

Method

All dsDNA models were generated from the http://structure.usc.edu/make-na/server.html server, and the BN nanosheet was modeled by using VDW software (version: 1.9.2beta1).[35] The BN parameters were adopted from a previous study.[36,37] Three different dsDNA sequences, poly(G–C, A–T)$_{20}$, poly(A–T)$_{40}$ and poly(G–C)$_{40}$, were used to explore the influence of the BN nanopore on various sequences. The dsDNA and BN were combined, and the first base pair was placed near the BN plane. To avoid any interaction of the BN nanosheet with its mirror system, all BNs were frozen in all simulations and had no gap with BNs related by mirror symmetry (in which no gap means BN boundary contacting to the BNs related by mirror symmetry directly). The size of every box used was set to 10.018 nm × 10.412 nm × 20.000 nm and each box was then filled with about 64 653 water molecules. Next, potassium ions were added into the solvated box to neutralize the charge of system. Meanwhile, 1 M KCl (1301 K^+ and 1301 Cl^-) was added in all systems. Other system details with various dsDNA sequences and different voltages used in each simulation are summarized in ESI,† Table S1.

The fully solvated complexes were then simulated with molecular dynamics (MD) simulations, which are widely used in the studies of biomolecules[38–44] and nanomaterials.[45–52] The MD simulations were performed with the software package GROMACS (version 4.6.6).[53] VMD software[35] was used to analyze and visualize the simulation results. We adopted the CHARMM 27 force field[54] and TIP3P water model[55] for the dsDNA and water molecules, respectively. The temperature was fixed at 300 K using a v-rescale thermostat and the volume of the simulation box was also kept constant during the simulation (*NVT*).[56] Periodic boundary conditions were applied in all directions. The long-range electrostatic interactions were treated with the PME method,[57] and the van der Waals (VDW) interactions were calculated with a cutoff distance of 1.0 nm. The geometrical properties of all solute bonds were kept constant at their equilibrium values with the LINCS algorithm,[58] and water geometry was also constrained using the SETTLE algorithm.[59] During the production runs, a time step of 2.0 fs was used, and data were collected every 4 ps.

Acknowledgements

We would like to thank Bruce Berne, Zaixing Yang, and Seung-gu Kang for helpful discussions. This work was partially supported by the National Natural Science Foundation of China (grant no. 11374221 and 11574224), the Priority Academic Program Development of Jiangsu Higher Education Institutions (PAPD). RZ acknowledges the support from IBM Blue Gene Science Program.

References

1 M. Gershow and J. Golovchenko, *Nat. Nanotechnol.*, 2007, **2**, 775–779.
2 J. J. Kasianowicz, E. Brandin, D. Branton and D. W. Deamer, *Proc. Natl. Acad. Sci. U. S. A.*, 1996, **93**, 13770–13773.
3 D. S. Talaga and J. Li, *J. Am. Chem. Soc.*, 2009, **131**, 9287–9297.
4 M. van den Hout, I. D. Vilfan, S. Hage and N. H. Dekker, *Nano Lett.*, 2010, **10**, 701–707.
5 B. M. Venkatesan, D. Estrada, S. Banerjee, X. Jin, V. E. Dorgan, M.-H. Bae, N. R. Aluru, E. Pop and R. Bashir, *ACS Nano*, 2011, **6**, 441–450.
6 J. Shendure and H. Ji, *Nat. Biotechnol.*, 2008, **26**, 1135–1145.
7 A. Singer, M. Wanunu, W. Morrison, H. Kuhn, M. Frank-Kamenetskii and A. Meller, *Nano Lett.*, 2010, **10**, 738–742.
8 B. McNally, A. Singer, Z. Yu, Y. Sun, Z. Weng and A. Meller, *Nano Lett.*, 2010, **10**, 2237–2244.
9 S. Garaj, W. Hubbard, A. Reina, J. Kong, D. Branton and J. Golovchenko, *Nature*, 2010, **467**, 190–193.
10 C. A. Merchant, K. Healy, M. Wanunu, V. Ray, N. Peterman, J. Bartel, M. D. Fischbein, K. Venta, Z. Luo and A. C. Johnson, *Nano Lett.*, 2010, **10**, 2915–2921.
11 J. A. Rodríguez-Manzo, M. Puster, A. Nicolaï, V. Meunier and M. Drndic, *ACS Nano*, 2015, **9**, 6555–6564.
12 B. Luan, J. Bai and G. Stolovitzky, *Appl. Phys. Lett.*, 2013, **103**, 183501.
13 S. Kesselheim, W. Mueller and C. Holm, *Phys. Rev. Lett.*, 2014, **112**, 018101.
14 B. Luan and G. Stolovitzky, *Nanotechnology*, 2013, **24**, 195702.
15 B. Luan, *Nanotechnology*, 2015, **26**, 055502.
16 C. Sathe, X. Zou, J.-P. Leburton and K. Schulten, *ACS Nano*, 2011, **5**, 8842–8851.
17 D. B. Wells, M. Belkin, J. Comer and A. Aksimentiev, *Nano Lett.*, 2012, **12**, 4117–4123.
18 S. Liu, B. Lu, Q. Zhao, J. Li, T. Gao, Y. Chen, Y. Zhang, Z. Liu, Z. Fan and F. Yang, *Adv. Mater.*, 2013, **25**, 4549–4554.

19 C. Peter and G. Hummer, *Biophys. J.*, 2005, **89**, 2222–2234.
20 M. G. Fyta, S. Melchionna, E. Kaxiras and S. Succi, *Multiscale Model. Simul.*, 2006, **5**, 1156–1173.
21 A. T. Guy, T. J. Piggot and S. Khalid, *Biophys. J.*, 2012, **103**, 1028–1036.
22 Y. Tu, M. Lv, P. Xiu, T. Huynh, M. Zhang, M. Castelli, Z. Liu, Q. Huang, C. Fan, H. Fang and R. Zhou, *Nat. Nanotechnol.*, 2013, **8**, 594–601.
23 Y. Zhang, C. A. Jimenez-Cruz, J. Wang, B. Zhou, Z. Yang and R. Zhou, *Sci. Rep.*, 2014, **4**, 7229.
24 R. Zhou, B. J. Berne and R. Germain, *Proc. Natl. Acad. Sci. U. S. A.*, 2001, **98**, 14931–14936.
25 R. Zhou, *Proc. Natl. Acad. Sci. U. S. A.*, 2003, **100**, 13280–13285.
26 R. Zhou, X. Huang, C. J. Margulis and B. J. Berne, *Science*, 2004, **305**, 1605–1609.
27 J. Li, X. Gong, H. Lu, D. Li, H. Fang and R. Zhou, *Proc. Natl. Acad. Sci. U. S. A.*, 2007, **104**, 3687–3692.
28 Y. Tu, H. Lu, Y. Zhang, T. Huynh and R. Zhou, *J. Chem. Phys.*, 2013, **138**, 015104.
29 Y. Tu, P. Xiu, R. Wan, J. Hu, R. Zhou and H. Fang, *Proc. Natl. Acad. Sci. U. S. A.*, 2009, **106**, 18120–18124.
30 C. Ge, J. Du, L. Zhao, L. Wang, Y. Liu, D. Li, Y. Yang, R. Zhou, Y. Zhao, Z. Chai and C. Chen, *Proc. Natl. Acad. Sci. U. S. A.*, 2011, **108**, 16968–16973.
31 A. G. Cherstvy, *J. Phys. Chem. B*, 2006, **110**, 14503–14506.
32 J. B. Heng, A. Aksimentiev, C. Ho, P. Marks, Y. V. Grinkova, S. Sligar, K. Schulten and G. Timp, *Nano Lett.*, 2005, **5**, 1883–1888.
33 B. Luan and A. Aksimentiev, *Phys. Rev. Lett.*, 2008, **101**, 118101.
34 W. Timp, U. M. Mirsaidov, D. Wang, J. Comer, A. Aksimentiev and G. Timp, *IEEE Trans. Nanotechnol.*, 2010, **9**, 281–294.
35 W. Humphrey, A. Dalke and K. Schulten, *J. Mol. Graphics*, 1996, **14**, 33–38.
36 C. Y. Won and N. R. Aluru, *J. Phys. Chem. C*, 2008, **112**, 1812–1818.
37 C. Y. Won and N. R. Aluru, *J. Am. Chem. Soc.*, 2007, **129**, 2748–2749.
38 R. H. Zhou, X. H. Huang, C. J. Margulis and B. J. Berne, *Science*, 2004, **305**, 1605–1609.
39 P. Liu, X. H. Huang, R. H. Zhou and B. J. Berne, *Nature*, 2005, **437**, 159–162.
40 M. Eleftheriou, R. S. Germain, A. K. Royyuru and R. Zhou, *J. Am. Chem. Soc.*, 2006, **128**, 13388–13395.
41 B. G. Fitch, A. Rayshubskiy, M. Eleftheriou, T. J. Christopher Ward, M. Giampaga, Y. Zhestkov, M. C. Pitman, F. Suits, A. Grossfield, J. Pitera, W. Swope, R. H. Zhou, S. Feller and R. S. Germain, *Blue Matter: Strong Scaling of Molecular Dynamics on Blue Gene/L*, Springer-Berlin, Heidelberg, 2006.
42 R. Zhou, P. Das and A. K. Royyuru, *J. Phys. Chem. B*, 2008, **112**, 15813–15820.
43 P. Das, J. A. King and R. Zhou, *Proc. Natl. Acad. Sci. U. S. A.*, 2011, **108**, 10514–10519.
44 P. Das, J. Li, A. K. Royyuru and R. Zhou, *J. Comput. Chem.*, 2009, **30**, 1654–1663.
45 Y. S. Tu, P. Xiu, R. Z. Wan, J. Hu, R. H. Zhou and H. P. Fang, *Proc. Natl. Acad. Sci. U. S. A.*, 2009, **106**, 18120–18124.
46 J. Y. Li, X. J. Gong, H. J. Lu, D. Li, H. P. Fang and R. H. Zhou, *Proc. Natl. Acad. Sci. U. S. A.*, 2007, **104**, 3687–3692.
47 P. Das and R. Zhou, *J. Phys. Chem. B*, 2010, **114**, 5427–5430.
48 C. Guo, Y. Luo, R. Zhou and G. Wei, *ACS Nano*, 2012, **6**, 3907–3918.
49 P. Xiu, Z. Yang, B. Zhou, P. Das, H. Fang and R. Zhou, *J. Phys. Chem. B*, 2011, **115**, 2988–2994.
50 G. H. Zuo, S. G. Kang, P. Xiu, Y. L. Zhao and R. H. Zhou, *Small*, 2013, **9**, 1546–1556.
51 Z. L. Gu, Z. X. Yang, Y. Chong, C. C. Ge, J. K. Weber, D. R. Bell and R. H. Zhou, *Sci. Rep.*, 2015, **5**, 9.
52 Z. L. Gu, Z. X. Yang, L. L. Wang, H. Zhou, C. A. Jimenez-Cruz and R. H. Zhou, *Sci. Rep.*, 2015, **5**, 11.
53 B. Hess, C. Kutzner, D. van der Spoel and E. Lindahl, *J. Chem. Theory Comput.*, 2008, **4**, 435–447.
54 A. D. Mackerell, M. Feig and C. L. Brooks, *J. Comput. Chem.*, 2004, **25**, 1400–1415.
55 W. L. Jorgensen, J. Chandrasekhar, J. D. Madura, R. W. Impey and M. L. Klein, *J. Chem. Phys.*, 1983, **79**, 926–935.
56 G. Bussi, D. Donadio and M. Parrinello, *J. Chem. Phys.*, 2007, **126**, 7.
57 D. J. Selkoe, *Physiol. Rev.*, 2001, **81**, 741–766.
58 B. Hess, H. Bekker, H. J. C. Berendsen and J. Fraaije, *J. Comput. Chem.*, 1997, **18**, 1463–1472.
59 S. Miyamoto and P. A. Kollman, *J. Comput. Chem.*, 1992, **13**, 952–962.